Enhanced Channel Estimation in RIS-Aided OFDM Systems Using DFT-Based Pilot Optimization under Practical Hardware Constraints

Donathe Uwingabire
Department of Electrical Engineering, Pan African University Institute for Basic Sciences, Technology and Innovation, hosted at Jomo Kenyatta University of Agriculture and Technology, Nairobi, Kenya
uwingabiredonathe17@gmail.com (corresponding author)

Stephen Kiambi
School of Electrical and Information Engineering, Jomo Kenyatta University of Agriculture and Technology, Nairobi, Kenya
skiambi@jkuat.ac.ke

Heywood Ouma Absaloms
Department of Electrical and Information Engineering, Faculty of Engineering, University of Nairobi, Nairobi, Kenya
houma@uonbi.ac.ke

Received: 10 March 2026 | Revised: 16 April 2026 | Accepted: 26 April 2026

Licensed under a CC-BY 4.0 license | Copyright (c) by the authors | *DOI: https://doi.org/10.48084/etasr.18638*

ABSTRACT

Reconfigurable Intelligent Surface (RIS) promises large spectral-efficiency gains for Orthogonal Frequency-Division Multiplexing (OFDM) systems but introduces significant channel-training challenges when the number of RIS elements grows. This paper proposes a practical, Discrete Fourier Transform (DFT)-based pilot optimization framework to reduce pilot overhead for channel estimation in RIS-aided OFDM links under realistic constraints, including finite RIS element counts and quantized phase shifts. Subsampled DFT pilots and sparse recovery reconstruct a truncated sparse delay-domain channel from a few measurements, greatly reducing pilot overhead while preserving estimation accuracy. Numerical results for a representative system size (N = 128) demonstrate significant reductions in pilot-symbol requirements compared to conventional full-dimensional training while maintaining estimation accuracy. Furthermore, conventional pilot overhead is observed to scale approximately linearly with RIS size, whereas the proposed scheme scales with the number of dominant channel coefficients. This paper analyzes trade-offs among Pilot Ratio (PR), measurement budget, and recovery performance, and provides guidelines for practical pilot-budget selection. The proposed approach is robust to quantized RIS phase shifts and offers improved spectral efficiency and latency benefits for large-scale RIS deployments. The study further highlights existing limitations, the need for ensemble-level validation, and directions for joint delay–angle sparsity exploitation and adaptive pilot allocation. This work introduces a low-complexity estimation method using DFT pilots and Least Squares (LS), accounting for quantized RIS phase shifts and frequency-selective fading. Evaluated through Normalized Mean Square Error (NMSE) and pilot overhead, the approach provides a scalable, practical solution for RIS-aided OFDM in next-generation networks.

Keywords-Reconfigurable Intelligent Surface (RIS); Orthogonal Frequency-Division Multiplexing (OFDM); Discrete Fourier Transform (DFT); Least Squares (LS)

I. INTRODUCTION

Reconfigurable Intelligent Surface (RIS) represents a major advancement in wireless communication, enabling intelligent control of signal propagation through passive reflecting elements that dynamically adjust phase and amplitude [1]. Unlike conventional active components, RIS can reshape the radio environment to enhance coverage, mitigate interference,

and improve energy efficiency, making it highly relevant for 6G and beyond networks [2, 3]. Orthogonal Frequency-Division Multiplexing (OFDM), widely adopted in 4G, 5G, and Wi-Fi networks, provides high spectral efficiency and resilience against multipath fading by dividing data into orthogonal subcarriers [4]. Integrating RIS with OFDM offers significant performance gains but introduces the challenge of cascaded channel estimation, since RIS elements cannot transmit or process signals directly. Accurate estimation is further complicated by frequency-selective fading, quantized phase shifts, and hardware constraints [5]. To address these issues, low-complexity methods, such as Discrete Fourier Transform (DFT)-based channel representations and optimized pilot designs, are increasingly being proposed [6].

Subsampled DFT pilots (including randomly selected subcarriers or time-frequency patterns) produce measurement matrices with favorable incoherence properties with respect to delay- or angle-domain sparsity bases, enabling accurate sparse recovery with far fewer measurements than dense, orthogonal training [7].

Several recent studies have investigated pilot design using Fourier-type sensing matrices and evaluated reconstruction performance with algorithms such as basis pursuit [8], Orthogonal Matching Pursuit (OMP) [9], Approximate Message Passing (AMP) for RIS [10], and massive Multiple-Input Multiple-Output (MIMO) channels subject to hardware limitations [11, 12].

Although several studies have investigated compressed sensing and sparse recovery techniques for RIS-assisted and massive MIMO systems, most existing works assume ideal continuous phase shifts and neglect pilot overhead under realistic hardware constraints. Furthermore, limited attention has been given to low-complexity Least Squares–Discrete Fourier Transform (LS–DFT) hybrid methods that balance performance and implementation cost. The impact of quantized RIS phase shifts and finite pilot budgets on channel estimation accuracy has not been sufficiently explored. This paper addresses these gaps by proposing a practical pilot optimization framework that explicitly considers hardware impairments and scalability.

II. SYSTEM AND CHANNEL MODELS

In Figure 1, the Base Station (BS) transmits the signal toward the RIS. The wireless channel between the BS and the RIS is represented by $H_{BR,k}$ where k denotes the OFDM subcarrier index. The RIS is composed of many passive reflecting elements whose phase shifts are controlled by a controller. By adjusting these phase shifts, the RIS can intelligently reflect the incoming signal toward the intended user.

After reflection from the RIS, the signal propagates through the RIS-to-User channel, denoted as $h_{RU,k}$ and finally reaches the User Equipment (UE). The tree in the diagram represents possible blockage in the direct BS-to-User path, which motivates the use of RIS to create a favorable reflected communication path.

Thus, the RIS assists the transmission by reconfiguring the wireless environment, improving signal strength and reliability. In an OFDM system, this process occurs across multiple subcarriers, and accurate channel estimation of the BS–RIS and RIS–User links is necessary for effective signal recovery at the receiver.

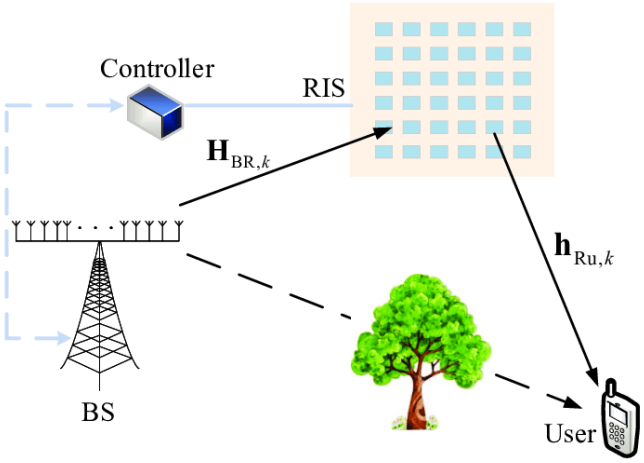

Fig. 1. Illustration of a downlink communication system for an RIS-aided OFDM network.

III. PROPOSED METHOD

This research employs a fundamental method to enhance channel estimation in RIS-aided OFDM systems using DFT-based sparse representation. In this work, the proposed DFT-based method estimates the effective cascaded channel under a fixed RIS configuration, rather than separately estimating the BS–RIS and RIS–UE channels. This assumption reduces training overhead and aligns with practical RIS implementations. This technique is specifically designed to operate within practical deployment constraints.

The first phase involves modeling the RIS-aided OFDM system under the following practical constraints. The system is structured with a single BS, a user terminal, and an RIS with N passive reflecting elements. The received signal, after reflection from the RIS, is expressed as follows [13]:

$$y[k] = H_{eff}[k]x[k] + n[k] \quad (1)$$

where $x[k]$ denotes the transmitted symbol, $n[k]$ represents Additive White Gaussian Noise (AWGN), and $H_{eff}[k]$ is the cascaded channel and is defined as:

$$H_{eff}[k] = h_{RU,k}\,\Phi H_{BR,k} \quad (2)$$

The matrix Φ represents the RIS reflection matrix that controls the phase shifts applied by the RIS elements. The RIS reflection matrix is given by:

$$\Phi = \mathrm{diag}\left(e^{j\theta_1}, \ldots, e^{j\theta_N}\right) \quad (3)$$

where θ_i $(i = 1,2, \ldots, N)$ represents the phase shift applied by the i-th RIS reflecting element, and N denotes the total number of RIS elements. The OFDM system is built with K

subcarriers, each with its own channel realization, in the presence of frequency-selective fading.

A. Discrete Fourier Transform–Based Channel Estimation

A DFT-based channel estimation algorithm is then implemented to exploit the sparse multipath nature of wideband OFDM channels in the delay domain. The Least Squares (LS) estimation is first applied using pilot symbols at the k-th OFDM subcarrier:

$$\widehat{H}_{LS}[k] = \frac{y_p[k]}{x_p[k]} \quad (4)$$

where $\widehat{H}_{LS}[k]$ is the estimated channel coefficient, $y_p[k]$ is the received pilot signal at the k-th subcarrier, and $x_p[k]$ is the known transmitted pilot symbol. The estimate is obtained by dividing the received pilot by the transmitted pilot symbol.

The time-domain channel tap estimate is obtained using the inverse DFT:

$$\hat{h}[n] = F^{-1}\widehat{H}_{LS}[k] \quad (5)$$

where $\hat{h}[n]$ represents the estimated channel impulse response in the delay domain at the n-th delay tap, and F^{-1} is the inverse DFT matrix. To reduce noise, only the significant taps are retained, whereas weaker taps are zeroed, exploiting the sparsity structure.

$$\hat{h}_{DFT}[n] = \begin{cases} \hat{h}[n], & n \le L_{max} \\ 0, & \text{otherwise} \end{cases} \quad (6)$$

The denoised frequency-domain estimate is recovered by applying the DFT as follows

$$\widehat{H}_{DFT}\,[k] = F\hat{h}_{DFT} \quad (7)$$

where $\widehat{H}_{DFT}$ denotes the reconstructed frequency-domain channel estimate obtained by applying the DFT to the denoised delay-domain channel vector $\hat{h}_{DFT}$, and L_{max} is the maximum channel delay spread, representing the number of significant multipath components. It is selected according to the assumed channel model and corresponds to the dominant channel taps retained during the sparsity-based reconstruction process. F in (7) represents the DFT matrix that transforms the signal from the delay domain to the frequency domain. This operation enhances robustness to noise and hardware impairments without increasing pilot overhead.

B. Pilot Optimization under Practical Constraints

To improve estimation efficiency, this stage optimizes pilot allocation across subcarriers. A pilot sequence matrix P is designed such that it minimizes the Normalized Mean Square Error (NMSE) while satisfying power and overhead constraints:

$$\min_{P} \text{NMSE} \text{ s.t. } \|P\|_0 \le P_{max} \quad (8)$$

where P denotes the pilot sequence matrix used for channel estimation, and NMSE is used as the optimization objective function. The term $\|P\|_0$ denotes the number of pilot symbols used, whereas P_{max} is the maximum allowed number of pilots. The optimization aims to design pilot sequences that minimize the estimation error while satisfying power and pilot overhead constraints.

C. Performance Evaluation and Comparative Analysis

The metrics used to evaluate the proposed algorithm are NMSE, Bit Error Rate (BER), and capacity, as defined below. The NMSE is given by:

$$\text{NMSE} = \frac{\|\widehat{H}-H\|^2}{\|H\|^2} \quad (9)$$

NMSE is used to measure the accuracy of the channel estimation algorithm, H denotes the true channel vector, and $\widehat{H}$ represents the estimated channel vector obtained from the estimation algorithm. The operator $\|\cdot\|$ denotes the Euclidean norm.

The BER denotes the bit error rate of the communication system and is given by:

$$\text{BER} = \frac{N_e}{N_b} \quad (10)$$

where N_e represents the number of bit errors and N_b represents the total number of transmitted bits.

The channel capacity is, by definition, given by:

$$C = \frac{1}{K}\sum_{k=1}^{K} \log_2\left(1 + \gamma\left|\widehat{H}[k]\right|^2\right) \quad (11)$$

Here C represents the channel capacity measured in bits per second per hertz (bps/Hz).

The Pilot Ratio (PR) is given by:

$$\text{PR} = \frac{P}{K} \quad (12)$$

The PR in the OFDM system is defined as the proportion of pilot subcarriers P relative to the total number of subcarriers K used in the transmission frame.

IV. RESULTS AND DISCUSSION

Comparisons between LS and DFT-based methods were conducted using the parameters listed in Table I. The simulation scenarios consider the number of RIS elements, quantized phase levels, PR, and fading models.

TABLE I. LIST OF PARAMETERS USED IN THIS STUDY

Parameter	Symbol	Value
RIS elements	N	128
RIS phase quantization bits	Q	2
Pilot Ratio	PR	1/8
Maximum channel delay spread	L_{max}	1, 2, 4, 8

The pilot design considers three key factors: pilot sparsity to reduce the number of subcarriers used, RIS phase quantization with discrete phase shifts $\theta_n \in \{0, \pi/2, 3\pi/2\}$, and time-varying channels, in which Doppler effects can disrupt subcarrier orthogonality. These considerations are made to ensure efficient pilot allocation while maintaining reliable channel estimation. Greedy selection and subcarrier grouping based on the channel coherence bandwidth are used to efficiently assign pilots.

Algorithm 1 summarizes the proposed LS and DFT-based channel estimation method for RIS-aided OFDM systems

```
Algorithm 1: LS and DFT-Based Channel
Estimation for RIS-Aided OFDM
Input:
    N = 128 (subcarriers)
    SNRdB_list = [0:5:30]
    pilotRatios = [1/8]
    L_br, L_ru = channel lengths
    Nsym = number of OFDM symbols
Output:
    NMSE vs SNR, BER vs SNR, Capacity vs
SNR
    Delay-domain sparsity profiles
    Pilot overhead vs BER
Algorithm:
1.  Initialize performance arrays:
     NMSE_LS, NMSE_DFT
     BER_LS, BER_DFT
     Capacity_LS, Capacity_DFT
2.  For each SNRdB in SNRdB_list:
     sigma2 ← 10^(-SNRdB/10)
2.1. For each pilotRatio in pilotRatios:
      P ← max(pilot_min, round(N *
      pilotRatio))
      pilotIdx ← evenly spaced indices
      dataIdx  ← remaining indices
2.2.  For each symbol in Nsym:
       Generate channel H with multipath
       taps
       Generate transmitted bits and
       modulate (BPSK)
       Insert pilots and data into OFDM
       symbol
       Add AWGN noise
       // LS estimation
       H_ls(pilotIdx) ← Y(pilotIdx)
       Interpolate remaining subcarriers
       // DFT estimation
       h_ls ← IFFT(H_ls)
       Select Lmax strongest taps (delay-
       domain sparsity)
       h_dft ← h_ls * mask
       H_dft ← FFT(h_dft)
       // Performance metrics
       NMSE_LS += ||H - H_ls||^2 / ||H||^2
       NMSE_DFT += ||H - H_dft||^2 /
       ||H||^2
       BER_LS += bit errors after
       detection with H_ls
       BER_DFT += bit errors after
       detection with H_dft
       Capacity_LS += mean(log2(1 +
       |H_ls|^2 * SNR))
       Capacity_DFT += mean(log2(1 +
       |H_dft|^2 * SNR))
2.3.  Average metrics over Nsym
3.  Plot results:
      - NMSE vs SNR (LS vs DFT)
      - BER vs SNR (LS vs DFT)
      - Capacity vs SNR (LS vs DFT)
      - Delay-domain sparsity (stem plots
        of |h_ls| vs |h_dft|)
      - Pilot overhead vs BER (LS vs DFT at
        fixed SNR)
End Algorithm
```

A. Normalized Mean Square Error vs Signal-to-Noise Ratio

Figure 2 illustrates the performance comparison of the LS and the proposed DFT method in terms of NMSE across varying Signal-to-Noise Ratio (SNR) levels. As shown, both estimation methods exhibit a decreasing NMSE (in dB) as SNR (in dB) increases. This trend is anticipated, as higher SNR values correlate with improved signal quality, thereby increasing the accuracy. The readings used to generate Figure 2 are shown in Table II for both LS and DFT across different L_{max} values.

Notably, the proposed DFT method yields lower NMSE values than the LS method when L_{max} is properly tuned. This suggests that the proposed DFT approach is more robust in environments characterized by lower signal strength and higher noise levels.

At elevated SNR levels, the NMSE of both methods levels off, but the DFT method continues to improve as L_{max} increases and eventually outperforms LS at $L_{max} \geq 4$ over the evaluation range. This consistent performance highlights the effectiveness of the DFT-based technique for channel estimation, showcasing its potential benefit in scenarios typically encountered in wireless communication systems.

The observed performance gain between the two methods underscores the advantages of the proposed DFT technique over conventional LS estimation, particularly under challenging conditions where accurate channel characterization is critical. The tendency of NMSE to decrease as SNR increases indicates improved estimation fidelity, making the DFT approach a compelling choice for applications integrating RIS. At low SNR, smaller L_{max} values are beneficial, as they filter noise and highlight dominant taps, yielding lower NMSE than LS. At higher SNR, however, the truncation discards useful channel energy, limiting estimation fidelity and reducing the advantage over LS. Thus, the optimal L_{max} depends on the operating SNR: smaller values are preferred in low-SNR regimes, whereas larger values are required to fully exploit high-SNR conditions.

TABLE II. NMSE VARIATION WITH L_{max} FOR LS AND DFT

SNR (dB)		0	5	10	15	20	25	30
L_{max} = 1	LS	-0.39	-0.39	-0.52	-0.56	-0.57	-0.58	-0.58
	DFT	-0.36	-0.38	-0.40	-0.39	-0.40	-0.40	-0.40
L_{max} = 2	LS	0.00	-0.39	-0.52	-0.56	-0.57	-0.58	-0.58
	DFT	-0.45	-0.49	-0.51	-0.51	-0.51	-0.50	-0.51
L_{max} = 4	LS	0.00	-0.39	-0.52	-0.56	-0.57	-0.58	-0.58
	DFT	-0.50	-0.57	-0.59	-0.59	-0.60	-0.59	-0.60
L_{max} = 8	LS	0.00	-0.39	-0.52	-0.56	-0.57	-0.58	-0.58
	DFT	-0.43	-0.57	-0.61	-0.62	-0.62	-0.62	-0.62

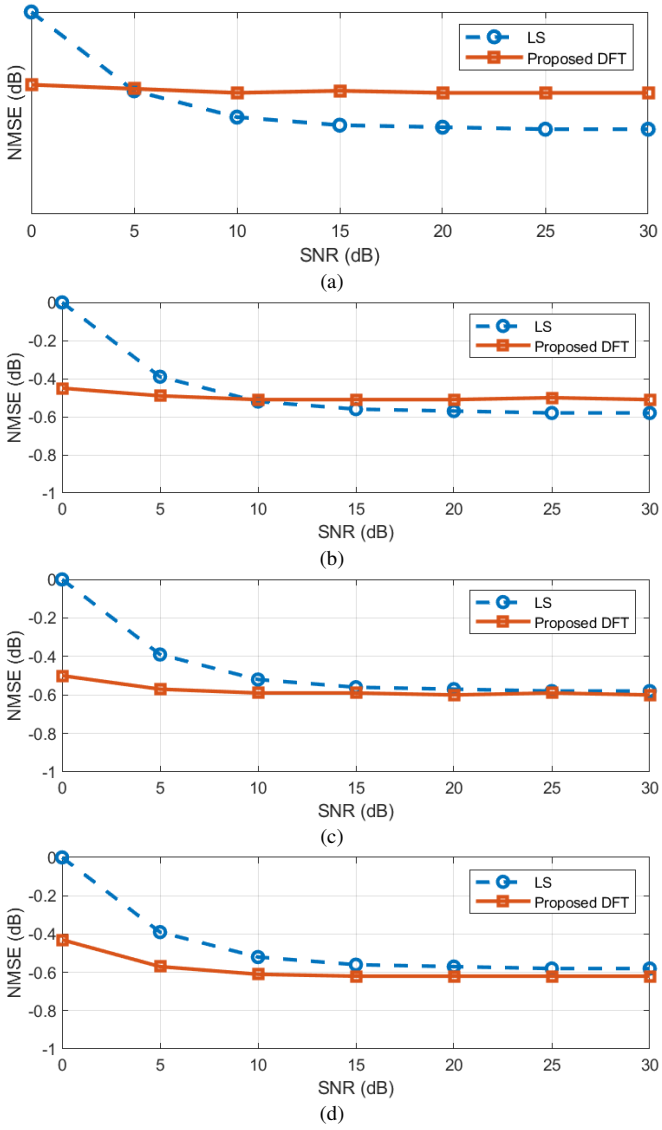

Fig. 2. NMSE comparison between LS and DFT for N = 128, Q = 2, PR = 0.125 for: (a) L_{max} = 1, (b) L_{max} = 2, (c) L_{max} = 4, (d) L_{max} = 8.

Increasing L_{max} by factors of 2, 4, and 8 allows the estimator to capture more channel energy. As SNR increases, the NMSE of the DFT decreases and eventually outperforms LS, emphasizing the importance of proper parameter tuning for high-SNR performance. LS, by contrast, assigns channel values directly at pilot positions without truncation or filtering, so its NMSE remains constant across SNR variations, driven mainly by pilot density and noise variance. In contrast, DFT benefits from selective noise suppression and energy retention.

B. Bit Error Rate vs Signal-to-Noise Ratio

Figure 3 presents the BER as a function of SNR. The plot reveals distinct performance trends for both methods across various SNR levels. Notably, in RIS-aided OFDM systems, the BER vs SNR results confirm that DFT-based estimation outperforms LS across all SNR levels.

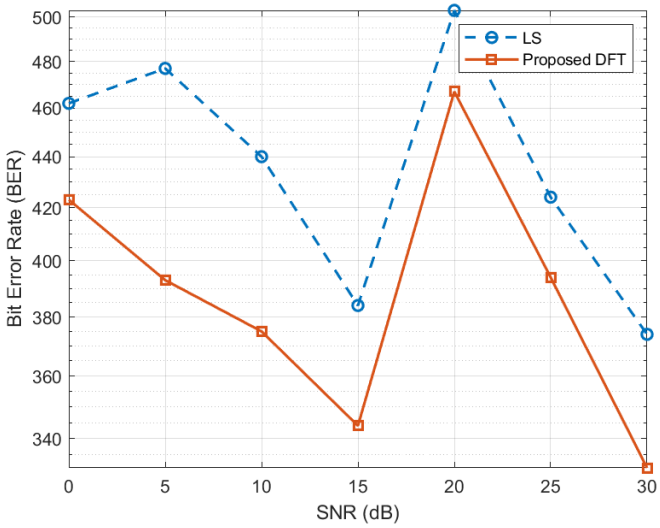

Fig. 3. BER vs SNR for N = 128, Q = 2, and PR = 0.125.

The DFT-based method achieves consistently lower BER and demonstrates more reliable performance across all SNR values, making it a more robust solution for RIS-aided OFDM systems. This validates the advantage of the DFT approach in practical deployments where both reliability and efficiency are critical.

At high SNR, both methods exhibit similar BER performance, signifying enhanced reliability under favorable channel conditions; however, the DFT-based method consistently demonstrates a lower error rate. This performance gain is attributed to its ability to exploit delay-domain sparsity and suppress noise more effectively.

Overall, these results reinforce the effectiveness of the DFT approach as a reliable and efficient solution for advanced wireless communication systems.

C. Capacity vs Signal-to-Noise Ratio

Figure 4 illustrates the relationship between channel capacity and SNR for the system under the specified parameters. The graph shows an increasing trend in channel capacity as SNR increases, demonstrating the positive correlation between SNR and capacity. This alignment is expected, as higher SNR values indicate a stronger signal relative to background noise, allowing for more efficient data transmission.

The capacity curves highlight that, while both LS and DFT estimators benefit from increasing SNR, the DFT-based estimator consistently achieves higher effective channel capacity. This is because the DFT approach suppresses noise and exploits delay-domain sparsity, yielding more reliable Channel State Information (CSI).

As a result, the capacity improvement of LS becomes less pronounced at moderate to high SNR levels, whereas DFT achieves more consistent capacity gains with increasing SNR. Importantly, tuning the DFT truncation length (L_{max}) ensures that sufficient multipath energy is retained, further boosting

capacity and reinforcing DFT's advantage in practical RIS-aided OFDM deployments.

This analysis underscores the importance of maintaining high SNR for optimal performance in communication systems, reinforcing the need for effective strategies to improve signal quality, particularly in environments where noise can significantly hinder performance. The findings validate the efficiency of the proposed system design and its potential for high-capacity applications in advanced communications technologies.

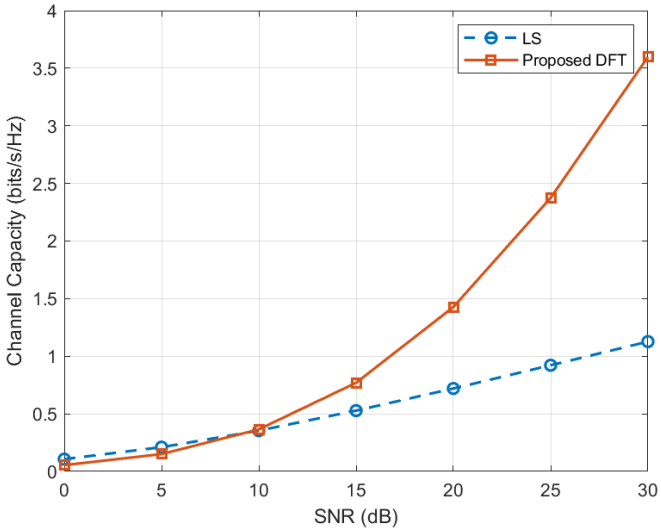

Fig. 4. Channel capacity comparison for LS and DFT.

D. Delay-Domain Sparsity

Figures 5 and 6 depict the magnitude of the estimated channel coefficients $|h[n]|$ against the corresponding delay indices. The concentration of channel power at specific delays suggests a sparse structure, in which a limited number of delay taps account for most of the channel's energy.

In particular, the sparse response indicates that LS estimation can be optimized, potentially reducing pilot overhead while maintaining estimation accuracy. The dominant taps can be exploited for improved performance in communication systems, enhancing both spectral efficiency and robustness against noise. The observed delay-domain sparsity in Figure 5 shows that LS distributes energy across many taps, reflecting both channel components and noise.

In contrast, Figure 6 shows that DFT-based processing concentrates energy into the dominant taps, revealing the underlying sparse structure of RIS-aided channels.

This behavior of wireless channels in the delay domain explains why the DFT method achieves better BER and capacity performance despite sometimes exhibiting higher NMSE. The configuration parameters (RIS size, quantization, and PR) primarily affect the amplitudes of dominant multipath components, whereas the overall sparsity structure and delay spread remain largely unchanged, confirming the robustness of sparse modeling for RIS-aided systems.

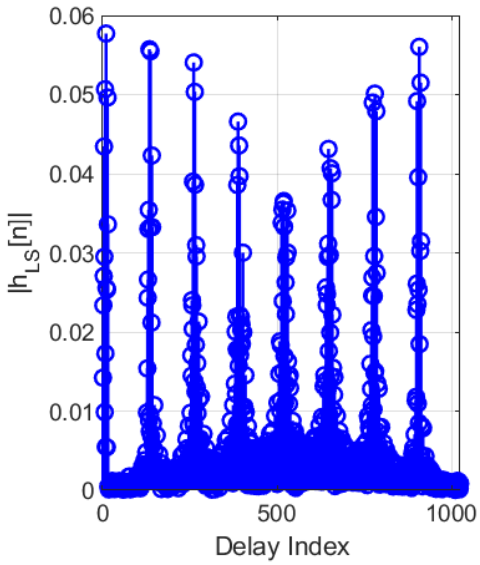

Fig. 5. Delay-domain sparsity of the estimated channel for LS.

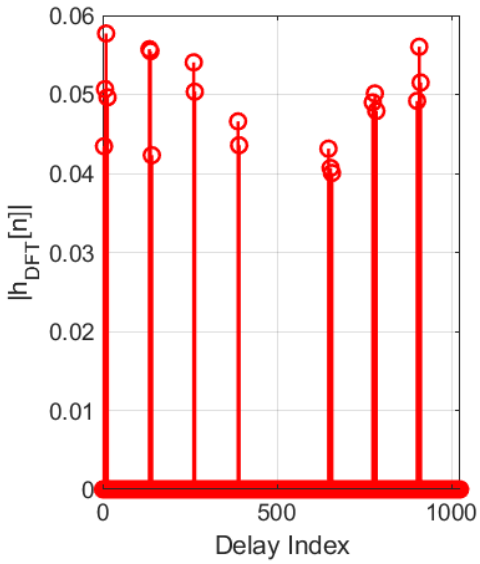

Fig. 6. Delay-domain sparsity of the estimated channel for the proposed DFT method.

E. Pilot Overhead Analysis for N = 128

For conventional LS channel estimation, the pilot overhead is determined by the need to estimate the full cascaded channel without exploiting sparsity. In this case, the required number of pilot symbols scales with the product of the number of subcarriers and the number of RIS elements and is given by:

$$P_{LS} = N \times K \quad (13)$$

where P_{LS} represents the pilot overhead for LS.

For the system parameters considered in this work (N = 128, K = 1,024), the pilot overhead becomes:

$$P_{LS} = 128 \times 1{,}024 = 131{,}072 \approx 13 \times 10^4$$

In Figure 7, the LS and the proposed DFT schemes are compared. It is shown that the conventional LS method requires a very large number of pilots (approximately 13×10^4), whereas the proposed DFT method requires only 0.248×10^4 pilots, which is significantly smaller. This indicates a substantial reduction in pilot overhead when using the DFT-based approach.

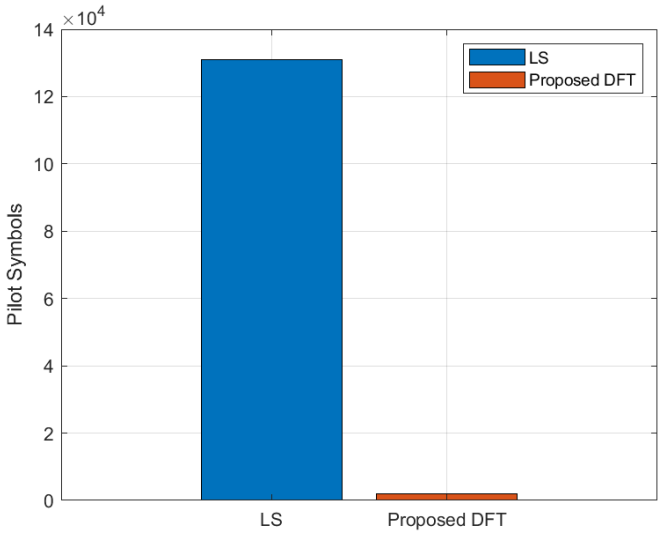

Fig. 7. Comparison of pilot overhead between LS and the proposed DFT method for N = 128 and PR = 0.125.

The implications of this reduction are profound: minimizing pilot overhead enhances spectral efficiency and contributes to overall system capacity. Furthermore, the reduced pilot requirements can lead to improved energy efficiency and prolonged battery life for mobile devices, which is a key consideration in modern communication systems.

Recent works, such as generative diffusion models for high-dimensional channel estimation [14] and diffusion model-based channel estimation for RIS-aided communication systems [15], achieve high estimation accuracy in terms of reduced NMSE and improved BER performance, particularly in complex and high-dimensional channel environments. However, these approaches typically require large training datasets and significant computational resources for both training and inference. In contrast, the proposed DFT-based method is model-driven and computationally efficient, achieving competitive performance without relying on training data. This makes it more suitable for real-time implementation and deployment in resource-constrained RIS-aided OFDM systems. The proposed DFT method demonstrates significant advantages in pilot overhead reduction, confirming its potential to optimize communication protocols in scenarios demanding high efficiency and performance.

V. CONCLUSION

The comparative evaluation of Least Squares (LS) and Discrete Fourier Transform (DFT)-based estimation in Reconfigurable Intelligent Surface (RIS)-aided Orthogonal Frequency-Division Multiplexing (OFDM) systems reveals consistent advantages of the proposed DFT-based framework across multiple performance dimensions.

Starting with Normalized Mean Square Error (NMSE) versus Signal-To-Noise Ratio (SNR), as SNR increases, the NMSE of the DFT-based method decreases and eventually outperforms LS, highlighting the importance of optimization for high-SNR performance. In terms of Bit Error Rate (BER) versus SNR, the results show that LS performance saturates as SNR increases, whereas the DFT-based method continues to improve, consistently achieving lower BER across the entire SNR range. This indicates that BER, as a key measure of end-to-end system reliability, favors the DFT-based approach even in scenarios where SNR performance alone may appear less favorable.

The capacity versus SNR analysis further demonstrates that the DFT-based method provides superior performance, particularly at low SNR. While the capacity achieved using LS tends to stagnate earlier due to its limited ability to handle noise, the DFT-based approach effectively translates improved channel estimation into higher throughput, scaling more efficiently with increasing SNR. A key factor behind these improvements is the exploitation of delay-domain sparsity. Delay-domain representations show that LS spreads energy across many taps, including noise components, whereas the DFT-based method concentrates energy on dominant channel taps, leading to more accurate and efficient channel representation.

Finally, the pilot overhead analysis for N = 128 shows that LS requires dense pilot allocation to maintain estimation accuracy, resulting in high overhead that scales poorly with the number of RIS elements. In contrast, the DFT-based method achieves better BER performance with significantly fewer pilots, thereby reducing overhead and allowing more resources to be allocated to data transmission.

Overall, the proposed DFT-based pilot optimization framework offers a practical solution for reducing pilot usage, minimizing spectral waste, and lowering energy consumption while maintaining robust channel estimation under realistic hardware constraints. By leveraging delay-domain sparsity, the approach achieves improved BER performance, higher capacity, and substantial pilot overhead reduction, supporting the deployment of RIS in next-generation wireless communication systems.

DECLARATION OF COMPETING INTERESTS

The authors declare that they have no competing interests.

ACKNOWLEDGMENT

The authors would like to acknowledge the African Union (AU) for its continued commitment to advancing research and innovation within Africa. This study received partial support from the African Union Commission, whose contribution provided essential resources for the development of this work.

DATA AVAILABILITY

The data generated and used in this study are described within the manuscript and no external datasets were used.

REFERENCES

[1] C. Pan *et al.*, "An Overview of Signal Processing Techniques for RIS/IRS-Aided Wireless Systems," *IEEE Journal of Selected Topics in Signal Processing*, vol. 16, no. 5, pp. 883–917, Aug. 2022, https://doi.org/10.1109/JSTSP.2022.3195671.

[2] Q. Wu and R. Zhang, "Towards Smart and Reconfigurable Environment: Intelligent Reflecting Surface Aided Wireless Network," *IEEE Communications Magazine*, vol. 58, no. 1, pp. 106–112, Jan. 2020, https://doi.org/10.1109/MCOM.001.1900107.

[3] W. Hussein, N. K. Noordin, K. Audah, M. F. B. A. Rasid, A. B. Ismail, and A. Flah, "Cascaded and Separate Channel Estimation based on CNN for RIS-MIMO Systems," *Engineering, Technology & Applied Science Research*, vol. 14, no. 3, pp. 14768–14774, June 2024, https://doi.org/10.48084/etasr.7499.

[4] H. F. Arrano and C. A. Azurdia-Meza, "OFDM: today and in the future of next generation wireless communications," in *2016 IEEE Central America and Panama Student Conference*, Guatemala City, Guatemala, 2016, pp. 1–6, https://doi.org/10.1109/CONESCAPAN.2016.8075209.

[5] X. Chen, T. Ling, J. Tian, Y. Han, and S. Jin, "Channel estimation in hybrid RIS-assisted MIMO OFDM systems independent of a Backhaul link," *Physical Communication*, vol. 71, Aug. 2025, Art. no. 102687, https://doi.org/10.1016/j.phycom.2025.102687.

[6] R. A. Roshdy and M. A. Salem, "A Proposed Channel Estimation Framework for Reconfigurable-Intelligent-Surface-Aided MIMO Communication System," *IEEE Internet of Things Journal*, vol. 10, no. 15, pp. 13612–13621, Aug. 2023, https://doi.org/10.1109/JIOT.2023.3262674.

[7] C. Qi, G. Yue, L. Wu, and A. Nallanathan, "Pilot Design for Sparse Channel Estimation in OFDM-Based Cognitive Radio Systems," *IEEE Transactions on Vehicular Technology*, vol. 63, no. 2, pp. 982–987, Feb. 2014, https://doi.org/10.1109/TVT.2013.2280655.

[8] N. Daryanavardan and A. Nosratinia, "Grid Mismatch in MmWave Sparse Channel Estimation: Analysis & Implications," in *ICC 2024 - IEEE International Conference on Communications*, Denver, CO, USA, 2024, pp. 5033–5038, https://doi.org/10.1109/ICC51166.2024.10622810.

[9] X. Wei, D. Shen, and L. Dai, "Channel Estimation for RIS Assisted Wireless Communications—Part II: An Improved Solution Based on Double-Structured Sparsity," *IEEE Communications Letters*, vol. 25, no. 5, pp. 1403–1407, May 2021, https://doi.org/10.1109/LCOMM.2021.3052787.

[10] Y. Guo *et al.*, "Efficient Channel Estimation for RIS-Aided MIMO Communications With Unitary Approximate Message Passing," *IEEE Transactions on Wireless Communications*, vol. 22, no. 2, pp. 1403–1416, Feb. 2023, https://doi.org/10.1109/TWC.2022.3204688.

[11] G. Interdonato, F. Di Murro, C. D'Andrea, G. Di Gennaro, and S. Buzzi, "Approaching Massive MIMO Performance With Reconfigurable Intelligent Surfaces: We Do Not Need Many Antennas," *IEEE Transactions on Communications*, vol. 73, no. 6, pp. 4000–4016, June 2025, https://doi.org/10.1109/TCOMM.2024.3506928.

[12] H. B. Mahesh, G. F. A. Ahammed, and S. M. Usha, "Design and Performance Analysis of Massive MIMO Modeling with Reflected Intelligent Surface to Enhance the Capacity of 6G Networks," *Engineering, Technology & Applied Science Research*, vol. 13, no. 6, pp. 12068–12073, Dec. 2023, https://doi.org/10.48084/etasr.6234.

[13] U. Mutlu, Y. Kabalci, and A. Cengiz, "Channel Estimation in RIS-aided Multi-User OFDM Communication Systems," in *2024 6th Global Power, Energy and Communication Conference*, Budapest, Hungary, 2024, pp. 765–770, https://doi.org/10.1109/GPECOM61896.2024.10582568.

[14] X. Zhou, L. Liang, J. Zhang, P. Jiang, Y. Li, and S. Jin, "Generative Diffusion Models for High Dimensional Channel Estimation," *IEEE Transactions on Wireless Communications*, vol. 24, no. 7, pp. 5840–5854, July 2025, https://doi.org/10.1109/TWC.2025.3549592.

[15] W. Tong, W. Xu, F. Wang, W. Ni, and J. Zhang, "Diffusion Model-Based Channel Estimation for RIS-Aided Communication Systems," *IEEE Wireless Communications Letters*, vol. 13, no. 9, pp. 2586–2590, Sept. 2024, https://doi.org/10.1109/LWC.2024.3431525.